PHOTONIC SENSORS / Vol. 7, No. 4, 2017: 350−356

Large Strain Detection of SRM Composite Shell Based on Fiber Bragg Grating Sensor

Lei ZHANG*, Xinlong CHANG, Youhong ZHANG, and Fan YANG

Xi'an Hi-Tech Institute, Xi'an, 710025, China

*Corresponding author: Lei ZHANG E-mail: lwzy_zl@163.com

Abstract: There may be more than 2% strain of carbon fiber composite material on solid rocket motor (SRM) in some extreme cases. A surface-bonded silica fiber Bragg grating (FBG) strain sensor coated by polymer is designed to detect the large strain of composite material. The strain transfer relation of the FBG large strain sensor is deduced, and the strain transfer mechanism is verified by finite element simulation. To calibrate the sensors, the tensile test is done by using the carbon fiber composite plate specimen attached to the designed strain sensor. The results show that the designed sensor can detect the strain more than 3%, the strain sensitivity is 0.0762 pm/με, the resolution is 13.13με, and the fitting degree of the wavelength-strain curve fitting function is 0.9988. The accuracy and linearity of the sensor can meet the engineering requirements.

Keywords: Composite material; large strain detection; fiber grating sensor

Citation: Lei ZHANG, Xinlong CHANG, Youhong ZHANG, and Fan YANG, "Large Strain Detection of SRM Composite Shell Based on Fiber Bragg Grating Sensor," *Photonic Sensors*, 2017, 7(4): 350–356.

1. Introduction

Solid rocket motor (SRM) health monitoring is a complex system that encompasses many projects. Damage detection of composite shell structures is one of the important aspects. Composites are subject to tensile strain, especially in quasi-static low strain rate tensile tests, some materials can even reach more than 10% [1]. T700 carbon fiber composite material 0° unidirectional composites stretch data show that the elongation of the composite at break is about 2%. Fiber optics is an enabling technology that offers definite advantages for embedding sensors into SRMs to measure stress, strain, pressure, and chemical properties. They are inherently safe since light is the only source of energy needed for the gages to function. The gages are very small and do not drift with time or require the same kind of calibration as electromechanical-type sensors [2]. However, the adoption of this technology in the historically conservative aerospace industry has been slow [3]. Fibers are typically made from brittle material such as glass, which are fragile and difficult to handle. The bare fiber long-term permissible strain in general is at 0.3% and no more than 1% in a short time [4]. Through a special strain transfer processing, the purpose of large strain can be achieved by using the glass fiber grating sensor.

At present, many scholars have studied the large strain detection technology based on fiber optic sensors. Huang *et al.* [5] achieved 2% strain measurement through the multi-mode interference polymer fiber. Kim *et al.* [6] used metal coated optical fiber sensors to determine the maximum

Received: 10 April 2017 / Revised: 30 July 2017

DOI: 10.1007/s13320-017-0423-3
Article type: Regular

strains experienced by composite structures. Ying *et al.* [7] presented an investigation into a new fabric strain sensor integrated with a looped polymeric optical fiber with V-shaped notches of large angle, which was capable of measuring repeated large strain up to 21%. Shen [8] achieved 54% strain measurement by folding arm structure. Wu *et al.* [9] transformed the measured strain into a small strain that the fiber grating could withstand by a composite structural substrate with a stainless steel annular flat spring, achieving a strain measurement greater than 2%. Huang *et al.* [10] designed a strain gauge platform for fiber grating sensors on which a fiber grating sensor with tube load was subject to a strain gauge greater than 0.5% in accordance with an equal load, and the scale factor of the platform load and strain was determined by k.

In this paper, based on the characteristics of fiber grating, a low-modulus substrate-mounted fiber grating sensor scheme for large strain measurement is designed. The test results show that it can detect at least 3% of the large strain and has high sensitivity and linearity.

2. Design of large strain sensor

2.1 FBG sensor package

In order to meet the requirement of measuring 3% (30000 με) large strain, it is necessary to redesign the traditional FBG sensor package structure. We package the FBG by poly-dimethylsiloxane (PDMS) which is a high molecular organic silicon compound having characteristics of optically transparent, non-toxic, hydrophobic, non-flammable, inert, and biocompatible, low-cost, and easy to use, therefore it has been widely used in microfluidic, bio-MEMS (micro-electro-mechanical systems), and other fields. In addition, PDMS also has low Young's modulus and high Poisson's ratio and other mechanical properties as well as high thermal expansion coefficient and thermal coefficient and other thermal properties. In this experiment, we mainly use the mechanical and thermal properties of PDMS to carry out the preparation of fiber optic sensors. The PDMS used in the present work is a liquid bi-component silicone pre-polymer, sylgard 184 manufactured by Dow Corning (Midland, MI). The PDMS rigidity can be controlled by the cross-linker agent concentration in the PDMS solution, the temperature, and the time of baking [11]. As the time and the temperature of baking are closely linked, we choose to bake the PDMS samples at a constant temperature of 100 ℃ (normal pressure conditions). The PDMS package for FBG is divided into the following steps:

(1) Fix the FBG. Place the FBG into the self-made Teflon mold (Fig. 1). The mold has a rectangular parallelepiped with a size of 40 mm × 6 mm × 1 mm. After the adjustment of the position of the FBG, fix its ends.

Fig. 1 Teflon mold.

(2) PDMS solution preparation. Mix the PDMS precursor and curing agent by 7.5 : 1 mass ratio, stir evenly, and put them into a vacuum oven to remove the bubbles in the PDMS solution.

(3) Cured package. Pour PDMS solution into the mold, put the mold into the incubator, set the temperature of 100 ℃, and bake 4 hours;

(4) Remove the mold. When the mold cools down to the room temperature, remove the mold. The packaged FBG is shown in Fig. 2.

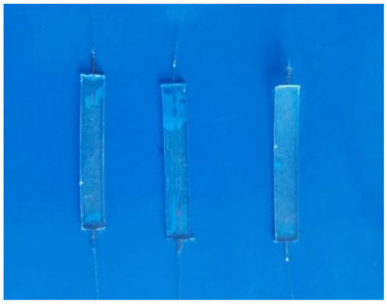

Fig. 2 Packaged FBG.

2.2 Strain transmission analysis

In order to meet the requirements of different strain measurements, different packaging materials and packaging parameters need to be selected. Therefore, it is necessary to obtain the qualitative relationship between the strain rate of the sensor and the parameters. Therefore, the strain transfer law of the sensor is analyzed. As Fig. 3 shows, the PDMS substrate length is $2L$, the width is b, the thickness is h_n, the thickness of upper substrate part of the fiber is h_c, the radius of the fiber is r_g, and the thickness of the adhesive layer is h_j.

The loading equilibrium and the geometric relation are obtained by using the axis symmetric model of the elastic free body in Fig. 4. As shown in diagram, the coordinate system's origin is placed at the center of the surface of substrate. σ_n, σ_g, and σ_j represent the substrate, the optical fiber, and the adhesive layer, respectively. τ_{ng}, τ_{nj}, and τ_{jm} respectively represent the shear stress substrate between fibers, substrate between adhesive layers, and substrate between matrices.

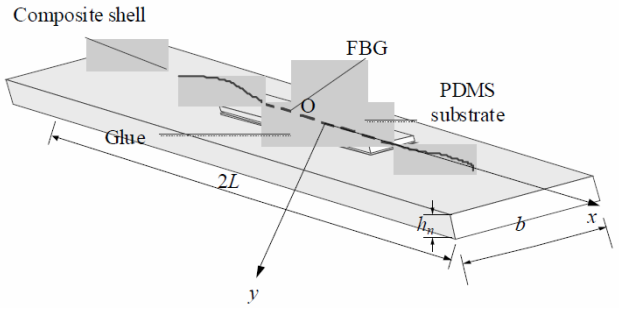

Fig. 3 Diagram of strain detection by coated FBG sensor.

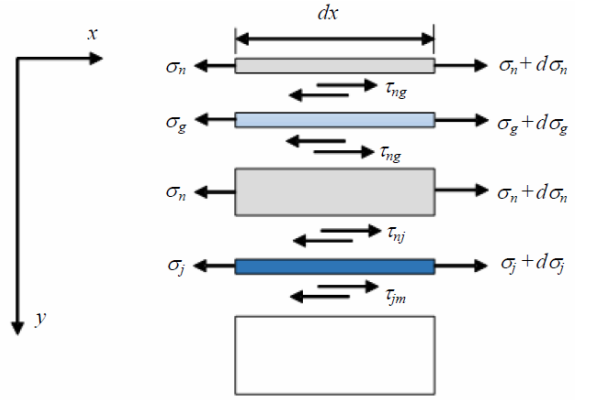

Fig. 4 Diagram of symmetrical section of the theoretical model loading equilibrium.

Along the x-axis on the substrate to take the micro-segment, the FBG sensor is subjected to force analysis. According to the loading equilibrium, the equation of FBG fiber can be obtained as follows:

$$d\sigma_g \pi r_g^2 = \tau_{ng} 2\pi r_g dx \tag{1}$$

which can be simplified as follows:

$$\tau_{ng} = \frac{r_g}{2}\frac{d\sigma_g}{dx}. \tag{2}$$

Similarly, the equation of FBG substrate is

$$d\sigma_n(bh_n - \pi r_g^2) + \tau_{ng} 2\pi r_g dx + \tau_{ng} b dx = 0 \tag{3}$$

which can be simplified as follows:

$$\frac{d\sigma_n}{dx} = \frac{-\tau_{nj} b - \tau_{ng} 2\pi r_g}{bh_n - \pi r_g^2}. \tag{4}$$

Substituting (4) into (2) yields:

$$\tau_{nj} = \frac{d\sigma_n(-bh_n + \pi r_g^2) - d\sigma_g \cdot \pi r_g^2}{dx \cdot b}. \tag{5}$$

The equation of FBG substrate adhesive layer is

$$d\sigma_j \cdot bh_j = (\tau_{nj} - \tau_{jm}) b dx \tag{6}$$

which can be simplified as follows:

$$\frac{d\sigma_j}{dx} = \frac{\tau_{nj} - \tau_{jm}}{h_j}. \tag{7}$$

Substituting (5) into (7) yields:

$$\tau_{jm} = \frac{d\sigma_n(\pi r_g^2 - bh_n) - d\sigma_g \cdot \pi r_g^2 - d\sigma_j \cdot bh_j}{bdx}$$

$$= -\left(h_n - \frac{\pi r_g^2}{b}\right)\frac{d\sigma_n}{dx} - \frac{\pi r_g^2}{b}\frac{d\sigma_g}{dx} - h_j\frac{d\sigma_j}{dx}. \tag{8}$$

It is assumed that the strain gradients of the layer are equal as follows:

$$\frac{d\varepsilon_g}{dx} = \frac{d\varepsilon_n}{dx} = \frac{d\varepsilon_j}{dx}. \tag{9}$$

Because the axial length of each layer is much larger than the radial dimension, the deformation is small, and the Poisson effect can be neglected, then we can get the following formula:

$$\frac{d\sigma_g}{dx} = E_g\frac{d\varepsilon_g}{dx}$$

$$\frac{d\sigma_n}{dx} = E_n\frac{d\varepsilon_n}{dx}$$

$$\frac{d\sigma_j}{dx} = E_j\frac{d\varepsilon_j}{dx}. \tag{10}$$

Substituting (10) into (8) yields:

$$\tau_{jm} = -E_g \frac{d\varepsilon_g}{dx}\left[\frac{E_n}{E_g}\left(h_n - \frac{\pi r_g^{\,2}}{b}\right) + \frac{\pi r_g^{\,2}}{b} + \frac{E_j}{E_g}h_j\right]. \quad (11)$$

Due to $E_g >> E_n$, $E_g >> E_j$, (11) can be simplified as follows:

$$\tau_{jm} = -E_g \frac{\pi r_g^{\,2}}{b} \cdot \frac{d\varepsilon_g}{dx}. \quad (12)$$

Similarly,

$$\tau_{nj} = -E_g\left[\frac{E_n}{E_g}\left(h_n - \frac{\pi r_g^{\,2}}{b}\right) + \frac{\pi r_g^{\,2}}{b}\right]\frac{d\varepsilon_g}{dx} \quad (13)$$

$$= -E_g \frac{\pi r_g^{\,2}}{b}\frac{d\varepsilon_g}{dx}$$

$$\therefore \tau_{jm} = \tau_{nj} \quad (14)$$

$$\tau_{ng} = \frac{E_g r_g}{2}\frac{d\varepsilon_g}{dx}. \quad (15)$$

Assume that the layers are all linear, the shear stress varies linearly with thickness, when $h_c + r_g \leqslant y \leqslant h_n$,

$$\tau_n = \frac{\tau_{nj}(y - r_g - h_c) + \tau_{ng}(h_n - y)}{h_n - h_c - r_g}$$

$$= \frac{\tau_{nj} - \tau_{ng}}{h_n - h_c - r_g}y + \frac{\tau_{nj}(-r_g - h_c) + \tau_{ng}h_n}{h_n - h_c - r_g} \quad (16)$$

and when $h_n \leqslant y \leqslant h_n + h_j$,

$$\tau_j = \frac{h_n + h_j - y}{h_j}\tau_{nj} - \frac{y - h_n}{h_j}\tau_{jm}$$

$$= \left(\frac{2h_n + h_j}{h_j} - \frac{2}{h_j}y\right)\tau_{nj}. \quad (17)$$

Ignoring the radial displacement of the adhesive layer and only considering the axial displacement, the following relationship can be given by

$$\tau_j = G_j \frac{du}{dy}.$$

Substituting (17) into the above equation and integrating of it yields

$$\int_{h_n}^{h_n+h_j} G_j \frac{du}{dy}dy = \int_{h_n}^{h_n+h_j}\left(\frac{2h_n + h_j}{h_j} - \frac{2}{h_j}y\right)\tau_{nj}dy \quad (18)$$

which is

$$G_j(u_m - u_j) = \left[2h_n + h_j - \frac{(h_n + h_j)^2 - h_n^{\,2}}{h_j}\right]\tau_{nj} = 0.$$

(19)

Differentiation of (19) with respect to x yields

$$\varepsilon_j = \varepsilon_m. \quad (20)$$

Similarly, for the substrate, $\tau_n = G_n \frac{du}{dy}$, substituting it into (16) and integrating it yields

$$\int_{h_j+r_g}^{h_n} G_n \frac{du}{dy}dy =$$

$$\int_{h_j+r_g}^{h_n}\left[\frac{\tau_{nj} - \tau_{ng}}{h_n - h_c - r_g}y + \frac{\tau_{nj}(-r_g - h_c) + \tau_{ng}h_n}{h_n - h_c - r_g}\right]dy \quad (21)$$

which is

$$G_n(u_j - u_n) = \frac{\tau_{nj} - \tau_{ng}}{2(h_n - h_c - r_g)}\left[h_n^{\,2} - (h_c + r_g)^2\right]$$

$$= \left\{-E_g \frac{\pi r_g^{\,2}}{b}\left[\frac{h_n^{\,2} - (h_c + r_g)^2}{2(h_n - h_c - r_g)} - h_c - r_g\right] - \frac{E_g r_g}{2}\left[\frac{h_n^{\,2} - (h_c + r_g)^2}{2(h_n - h_c - r_g)} - h_n\right]\right\}\frac{d\varepsilon_g}{dx}$$

$$= E_g(A + B)\frac{d\varepsilon_g}{dx} \quad (22)$$

where

$$A = -\frac{\pi r_g^{\,2}}{b}\left[\frac{h_n^{\,2} - (h_c + r_g)^2}{2(h_n - h_c - r_g)} - h_c - r_g\right]$$

$$B = -\frac{r_g}{2}\left[\frac{h_n^{\,2} - (h_c + r_g)^2}{2(h_n - h_c - r_g)} - h_n\right].$$

Differentiation of (22) with respect to x yields

$$\varepsilon_n = \varepsilon_j + \frac{1}{k^2}\frac{d^2\varepsilon_g}{dx^2} \quad (23)$$

where

$$\frac{1}{k^2} = \left|\frac{E_g}{G_n}(A + B)\right|. \quad (24)$$

Equation (23) can be written as

$$\frac{d^2\varepsilon_g}{dx^2} - k^2\varepsilon_g + k^2\varepsilon_m = 0 \quad (25)$$

of which the general solution is

$$\varepsilon_g(x) = C_1 e^{kx} + C_2 e^{-kx} + \varepsilon_m \quad (26)$$

where C_1 and C_2 are the integration constants determined by the boundary condition.

Since the intersection of the fiber end between the substrate and adhesive layer is free, the boundary conditions are given by

$$\varepsilon_g(L)=\varepsilon_g(-L)=0$$

which can be obtained as

$$C_1=C_2=-\frac{\varepsilon_m}{2\cosh(kL)}. \tag{27}$$

The solution of (26) is (28), which is the distribution strain of FBG sensor in axis direction:

$$\varepsilon_g(x)=\varepsilon_m\left[1-\frac{\cosh(kx)}{\cosh(kL)}\right] \tag{28}$$

where $\varepsilon_g(x)$ is the strain of fiber in axial direction, and ε_m is the strain produced by matrix in the axial direction. The detection area can be regarded as suffering from a uniform strain due to the module, and the size of the matrix structure is larger than substrate's. The strain detected by FBG sensor is average strain on substrate in practical use, which is

$$\begin{aligned}\overline{\varepsilon_g}&=\frac{2\int_0^L[1-\cosh(kx)/\cosh(kL)]\mathrm{d}x}{2L}\\&=\left[1-\frac{\sinh(kL)}{kL\cosh(kL)}\right]\varepsilon_m.\end{aligned} \tag{29}$$

The average coefficient of the reactions and transfers of the sensor is

$$\overline{\alpha}=\frac{\varepsilon_m}{\overline{\varepsilon_g}}=\frac{1}{1-\sinh(kL)/[kL\cosh(kL)]}. \tag{30}$$

3. Finite element method verification

In order to further verify the above-mentioned strain transfer analysis, a three-dimensional model of the design scheme is established in commercial software ABAQUS, and the finite element simulation of the working process is carried out. The finite element model and grid division are shown in Fig. 5. As the bottom of the sensor substrate is thin and the modulus is close to the substrate, the model is simplified to three parts: the tensile specimen, the substrate, and the fiber, and the specific parameters of each part are shown in Table 1 [12, 13].

The boundary condition of the model uses the displacement constraint to give a 1-mm displacement perpendicular to the cross section in the axial cross section of the tensile specimen to simulate the case where the tensile specimen produces a 2% strain. The tensile specimen between the substrate and the contact surface between the substrate and the optical fiber is bound by using a binding. The results of the cloud and fiber axial strain curves are shown in Fig. 6.

Table 1 Parameters of layers.

Fiber	Young's modulus, E (MPa)	72 000
	Possion's ratio, v	0.17
	Size (mm)	30 × ϕ0.125
Substrate	Young's modulus, E (MPa)	4
	Possion's ratio, v	0.497
	Size (mm)	40 × 6 × 1
Carbon fiber composite	Young's modulus, E (unidirectional) (MPa)	105 000
	Possion's ratio, v	0.3
	Size (mm)	100 × 12 × 2

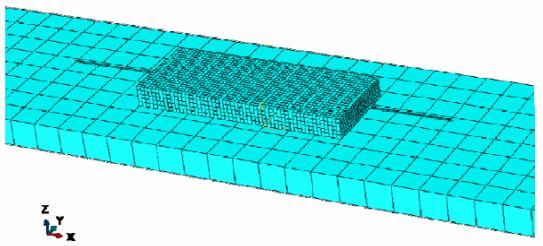

Fig. 5 Finite element model and grid division.

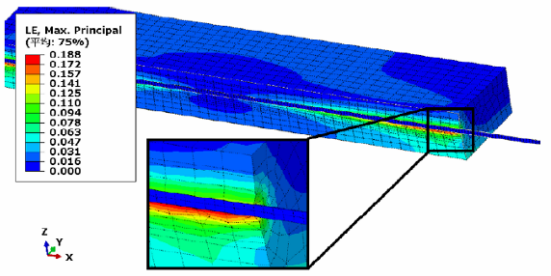

Fig. 6 Profile strain cloud.

From the above strain cloud and curve, the input strain of the tensile specimen is 2%, and the maximum strain of the optical fiber is 0.147%, which is less than 0.3% of the long-term use of silica fiber, and the central strain transfer coefficient is 13.6. The average strain transfer coefficient of the embedded part of the optical fiber is 21.3, which indicates that the low modulus elastic substrate can be a good transition of the tensile strain to the small strain of the fiber. As can be seen from Fig. 7, the maximum strain of the substrate occurs at the junction of the two ends with the optical fiber, reaching 18.8%, and the end face is recessed by the fiber, so the fiber debonding is also the first to occur here.

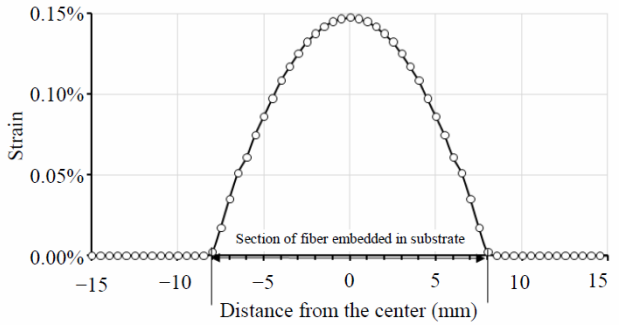

Fig. 7 Axial stain curve of fiber-optical.

4 Test on carbon fiber composite

The designed sensor is tested by the tensile test on a carbon fiber composite plate. The experiment is carried out on the CMT5205 material testing machine. The tensile test piece is made of carbon fiber composite material, and the effective size is 130 mm × 15 mm × 2 mm. The coated fiber grating sensor and the high-precision resistance strain gauge extension specimen are arranged in the direction of stretching, then the adhesive is attached to the tensile specimen by 502 glue, and the central wavelength of the grating is 1550.500 nm. The monitoring system of tensile test is shown in Fig. 8.

Fig. 8 Monitoring system of tensile test.

According to the basic principle of fiber grating, the strain coefficient of Bragg grating near 1550 nm is 1.209 pm/με [14]. Ignoring the temperature change during the experiment, the actual strain of the FBG can be obtained though dividing the wavelength variation of the FBG sensor by the strain coefficient. Fig. 8 depicts the contrast of the carbon fiber composite's strain measured by the strain gauge and FBG sensor.

The actual strain on the surface of the carbon fiber composite was measured as shown in Fig. 9. According to the fitting formula, the strain transfer coefficient of FBG large strain sensor is obtained as follows:

$$\alpha_1 = \frac{\varepsilon_y}{\varepsilon_g} = \frac{\sigma_g'}{\sigma_y'} = \frac{2115936.7975}{124984.7397} = 16.04 .$$

The strain measured by the high-precision resistance strain gauge is taken as the abscissa, and the FBG central wavelength change of the fiber grating demodulator is taken as the vertical axis to obtain the wavelength-strain curve as shown in Fig. 10.

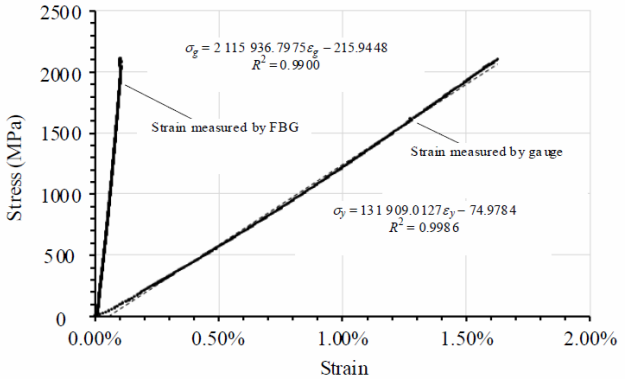

Fig. 9 Strain contrast of fiber Bragg grating and stain gauge.

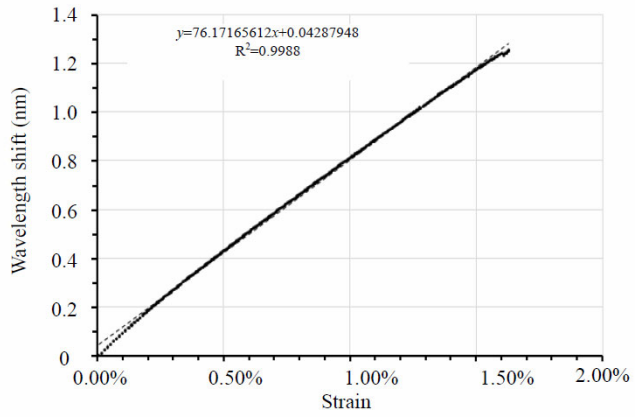

Fig. 10 Wavelength-strain curve of the sensor.

We can see from the wavelength-strain curve that there is a good linearity between the two variables. The linear fitting function of wavelength-strain is as follows:

$$y = 76.17165612x + 0.04287948$$

the linear degree of fit is as follows:

$$R^2 = 0.9988 .$$

and the sensor average sensitivity is as follows:

$$S_2 = \left|\frac{\Delta\lambda}{\Delta\varepsilon}\right| = 76.17165612\,\text{nm}/\varepsilon = 0.0762\,\text{pm}/\mu\varepsilon$$

so the resolution is 13.13 με.

5. Conclusions

In this paper, the silica optical FBG strain sensor with a polymer package is redesigned to test the larger strain on carbon composite of SRM shell. The strain transfer function of the sensor is deduced. Based on the finite element simulation analysis of the three-dimensional model, it is verified that the strain transfer mechanism is correct. At last, the tensile test on the carbon fiber composite plate fixing the FBG large strain sensor is made and the detection to the calibration is made by the resistance strain gage of high precision. The strain rate of the sensor is 16.04, and the strain sensitivity is 13.13 με, which indicates that the sensor could meet the requirements of the detection. According to the analysis of experimental data, the large strain packaging scheme designed in this paper has a good detection effect on carbon fiber composites, and its range can meet the requirements of carbon fiber composite strain test.

Acknowledgment

The paper is financially supported by the National Scientific Support program of China (Grant No. 51605480).

References

[1] Z. H. Wang, G. P. Zhao, J. F. Ma, and J. X. Zheng, "Experiment study on the strain rate behavior of carbon/epoxy composite materials," *Acta Materiae Compositae Sinica*, 2007, 24(2): 113–119.

[2] R. S. Hyde, "A solid rocket motor manufacturer's view of sensors and aging surveillance," in *Proc. of 37th Joint Propulsion Conference and Exhibit*, Salt Lake City, 2001.

[3] C. Davis, S. Tejedor, I. Grabovac, J. Kopczyk, and T. Nuyens, "High-strain fiber Bragg gratings for structural fatigue testing of military aircraft," *Photonic Sensors*, 2012, 2(3): 215–224.

[4] S. D. Siberstein, R. B. Lipton, S. Solomon, and N. T. Mathew, "Classification of daily and near-daily headaches: proposed revisions to the IHS criteria," *Headache the Journal of Head and Face Pain*, 1994, 34(1):1–7.

[5] J. Huang, X. W. Lan, H. Z. Wang, and H. Xiao, "Polymer optical fiber for large strain measurement based on multimode interference," *Optics letters*, 2012, 37(20): 4308–4310.

[6] S. W. Kim, M. S. Jeong, I. Lee, E. Kim, I. B. Kwon, and T. K. Hwang, "Determination of the maximum strains experienced by composite structures using metal coated optical fiber sensors," *Composites Science and Technology*, 2013, 78: 48–55.

[7] D. Q. Ying, X. M. Tao, W. Zheng, and G. F. Wang, "Fabric strain sensor integrated with looped polymeric optical fiber with large angled v-shaped notches," *Smart Materials and Structures*, 2013, 22(1): 1–11.

[8] X. Y. Shen, "Study on the strain sensing and its enlarging technology based on fiber grating," Ph.D. dissertation, Tianjin University, Tianjin, China, 2010.

[9] J. Wu, H. P. Wu, J. B. Huang, and H. C. Gu, "Large range FBG sensor for ship structure health monitoring," *Optics and Precision Engineering*, 2014, 22(2):311–317.

[10] J. Huang, C. W. Liu, D. Wei, and L. I. Meng, "Discussion on large strain calibration method using FBG sensor," *Equipment Environmental Engineering*, 2013, 10(4): 86–89.

[11] D. Fuard, T. Tzvetkova-Chevolleau, S. Decossas, P. Tracqui, and P. Schiavone, "Optimization of poly-di-methyl-siloxane (PDMS) substrates for studying cellular adhesion and motility," *Microelectronic Engineering*, 2008, 85(5–6): 1289–1293.

[12] K. T. Wan, C. K. Y. Leung, and N. G. Olson, "Investigation of the strain transfer for surface-attached optical fiber strain sensors," *Smart Materials and Structures*, 2008, 17(3):1–12.

[13] L. Sun, C. Y. Yue, and Y. S. Song, "Strain transfer analysis of substrate fiber Bragg grating sensor," *Journal of Optoelectronics Laser*, 2013, 24(5): 849–854.

[14] W. W. Morey, G. Meltz, and W. H. Glenn, "Fiber optic Bragg grating sensors," *SPIE*, 1990, 1169(96): 98–107.